



The *in vitro* photodynamic activity, photophysical and photochemical research of a novel chlorophyll-derived photosensitizer

Guanghai Tan¹ · Qi Wang² · Hongyue Zhang² · Jianjun Cheng² · Zhiqiang Wang² · Fengyu Qu^{1,2} · Changhong Guo¹ · Yingxue Jin²

Received: 22 February 2017 / Accepted: 14 June 2017 / Published online: 3 July 2017
© Springer Science+Business Media, LLC 2017

Abstract Chlorophyll has always been used as the leading compound for photodynamic therapy drug development. In this paper, a novel methyl pyropheophorbide-a- derived photosensitizer, 3-acetyl-3-devinyl-13¹-dicyanomethylene-pyropheophorbide-a was synthesized through modifications at C-13¹, C-3, and C-17 positions of methyl pyropheophorbide-a. The compound exhibited a longer wavelength absorption at 713 nm (in methanol) than that of methyl pyropheophorbide-a (667 nm) due to the enlarged the aromatic conjugation system by dicyanomethylene, allowing it to be potential in deep tumor treatment. Moreover, benefiting from the carboxylic group at C-17 and the acetyl group at C-3, the title compound was endowed with better water solubility than that of methyl pyropheophorbide-a. Detailed *in vitro* photodynamic therapy research showed ADCPPa could be uptaken by cancer cells successfully and killed the cancer cells more efficiently than the leading compound methyl pyropheophorbide-a under light (light dose 10 J/cm²) due to the high singlet oxygen quantum yield (65.98%). The excellent anti-photobleaching ability (degradation rate 1.6% in 10 min) also boosted its potential in practical application. In addition, the research has disclosed that during photochemical

processes of photodynamic therapy, the formation of singlet oxygen after photodynamic therapy treatment played a major role, comparing with the formation of superoxide anion and radicals. Finally, the real time quantitative polymerase chain reaction (RT-qPCR) experiments have showed that the target compound has important regulating effect on expression of CDK2 and Survivin, consequently leading to apoptosis and cell death.

Keywords Photodynamic therapy · Methyl pyropheophorbide-a · Dicyanomethylene · Antitumor

Introduction

Photodynamic therapy (PDT) is a clinically approved and minimally invasive therapeutic procedure to cancer treatment because of the low toxicity without light irradiation, the selective toxicity to the multiple lesions upon irradiating, and the ability to retreat a tumor during various therapeutic methods (Cabuy 2012). PDT involves the administration of a photosensitizer (PS) followed by illumination of the tissue with visible light. After administrations of a drug and upon the absorption of appropriate light, a PS is excited from ground state (S_0) to the first excited state with the same spin multiplicity (S_1). Then, the excited PS can decay to the S_0 state by losing its energy through emitting fluorescent light or converting into heat by radiation-less internal conversion. Alternatively, the first excited state S_1 can be converted into electronic spin triplet (T_1). From T_1 state, the PS can return to the S_0 state by emitting phosphorescence. If this state (T_1) has a sufficient long life and the process occurs in the presence of molecular

✉ Fengyu Qu
quprof@163.com

✉ Changhong Guo
guoprof@163.com

✉ Yingxue Jin
jyxprof@163.com

¹ College of Life Science and Technology, Harbin Normal University, Harbin 150025, China

² College of Chemistry & Chemical Engineering, Harbin Normal University, Harbin 150025, China

oxygen or water, it can generate superoxide anions and radical intermediate species (type I reaction) or transfer energy to the oxygen ($^3\text{O}_2$) to produce active singlet oxygen ($^1\text{O}_2$) (type II reaction) (Fig. 1) (Cabuy 2012; Phillips 2010), which are responsible for damage to cancer cells. It is generally accepted that type I reaction and type II reaction can occur simultaneously and $^1\text{O}_2$ generated from a type II reaction is the principal cytotoxic component in PDT (Noimark et al. 2013).

Despite the advantages of PDT (minimum side effects, low toxicity to tissues without light, non-invasive therapy and high selectivity), its application in clinic is always restricted to peripheral and endoscope accessible tissues (Agostinis et al. 2011; Lu et al. 2014; Sosnik and Carcaboso 2014; Volgger and Betz 2016), because PDT for deep tumors is limited by the tissue penetration depth of excitation light (Yoon et al. 2014; Voon et al. 2014). Generally, the reasonable tissue penetration depth is achieved with irradiation light wavelengths in the range of 650–900 nm (NIR window) (Hu et al. 2015). It is acknowledged that developing the PS with longer wavelength of maximum absorption is of significance for treatment of deep tumor, for light with longer wavelength will penetrate deeper into tissues than the light with shorter wavelength (Payne et al. 1996).

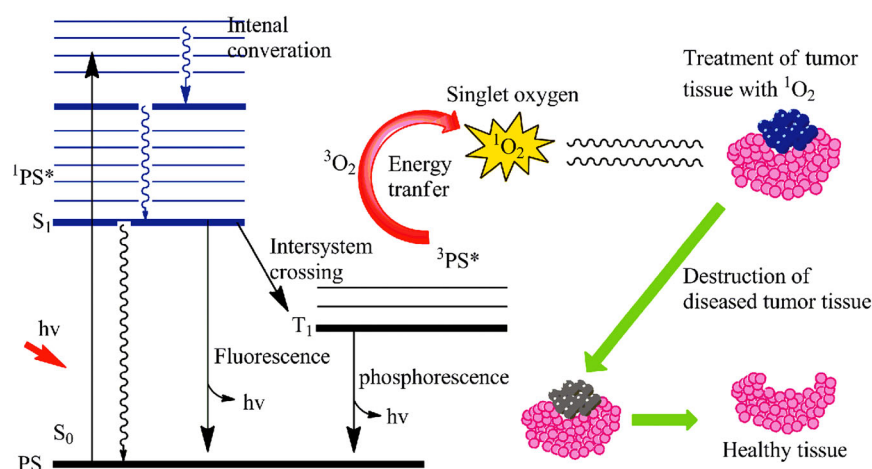
Many researchers have focused on developing novel PS derivatives with large absorbance in the NIR window to fight against deep tissue cancers (Wan et al. 2014; Guo et al. 2014; Tuncel et al. 2013; Yang et al. 2013). Currently, the most common PSs in clinic are porphyrins and their derivatives, such as the first generation PSs hematoporphyrin derivative (HpD) and Photofrin (with a maximal absorption at 630 nm); the second generation PSs Foscan, Npe6, Lutex, Verteporfin, Purlytin and Tookad (O'Connor et al. 2009). Because of the low dark cytotoxicity, being prone to accumulate in tumor lesions, strong absorption around the NIR window and high singlet oxygen yield, the porphyrin

PSs have attracted wide attention for medical application. The natural porphyrins (chlorins) in plants, chlorophylls, are extremely important biomolecules in photosynthesis, which allow plants to absorb solar radiation, converting light energy into chemical energy. The four pyrrole subunits interconnected via methane bridges construct a conjugated 18- π electron macrocycle, which gives rise chlorophyll strong absorption at the range of 600–700 nm and high singlet oxygen quantum yield, making them 'hot' molecules in PS research (Liu et al. 2015; Zhang et al. 2014; Asano et al. 2013).

Because of inhomogeneous electric charge distribution of the multi- π aromatic system caused by the asymmetrical chemical structure of chlorophylls, and the active chemical properties resulted from the exocyclic nonaromatic unsaturated substituents, such as carbonyl or vinyl group, chlorophylls are moderately easy and feasible for structural modifications. The variety of chlorin derivatives can be obtained by modifying peripheral substituted group, and C-3, 5, 7, 10, 12, 13, 17 and 20 positions are highly active reactive sites and are easily modified for development of new PSs (Li et al. 2015; Smith et al. 1985; Han et al. 2001; Li et al. 2016, 2014; Staron et al. 2015). Generally, good PSs in PDT should possess large absorption wavelength and rational water-soluble ability for practical use. Porphyrinic methyl pyropheophorbide-a (MPPa), which is a semisynthetic PS derived from chlorophyll *a*, has been used as the leading compound in many structural modifications of medicinal chemistry, due to the advantages of long absorption wavelength (>667 nm), low dark cytotoxicity and high singlet oxygen quantum yield (Eichwurz et al. 2000; Sun and Leung 2002).

In the present study, a MPPa-derived PS, 3-acetyl-13¹-dicyanomethylene- pyropheophorbide-a (ADCPPa) was synthesized through modification at C-13¹ position of Mppa with dicyanomethylene to extend the absorption maximum in the near-infrared spectral region (Qy absorption),

Fig. 1 Photochemical process and the bioaction mechanism of photosensitizer



allowing the PS to be potential in deep tumor treatment. (Scheme 1) (Vail et al. 2014). Meanwhile, the methyl propionate moiety at C-17 position was hydrolyzed into propionic acid group, and the vinyl group at C-3 group was oxidized into acetyl group, both leading to a better water solubility. Although modification by dicyanomethylene at C¹³ position has been reported (Wang et al. 2012), yet those C-17 ester-hydrolyzed compounds of dicyanomethylene-modified derivatives have not been reported, and the detailed photophysical and photochemical properties, the antitumor activities and photochemical mechanism have not been investigated systematically. In the present paper, a comprehension research for ADCPPa, including the UV–Vis and fluorescence spectral properties, the singlet oxygen yield, the anti-photobleaching ability, the in vitro photocytotoxicity against HeLa cells, the cancer cell uptaking behavior, and the morphological changes of cancer

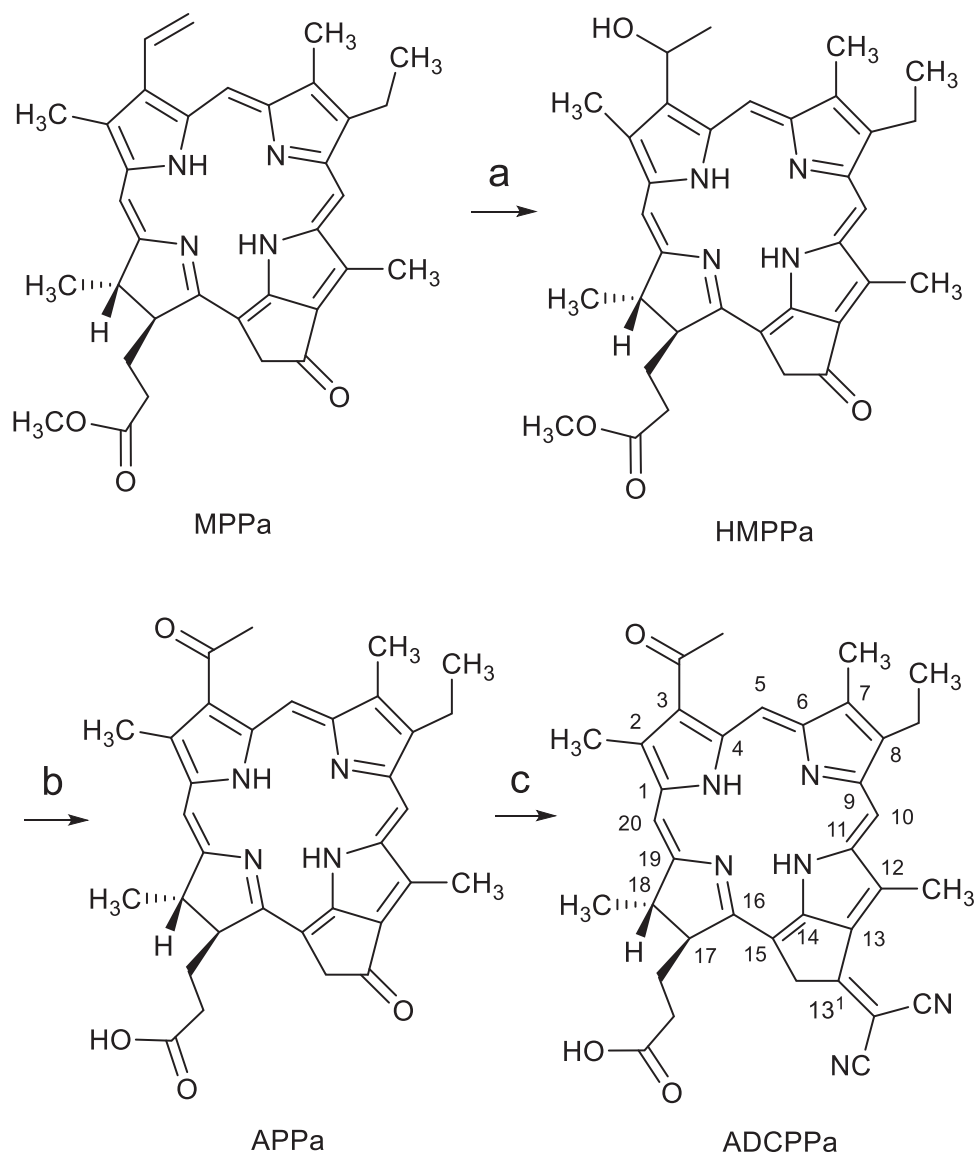
cells after drug treatment, were all investigated to evaluate the title compound in support of PDT. In addition, the photochemical mechanism in PDT was investigated by using D-mannitol (DM) and sodium azide (SA) as quenching agents of reactive oxygen species (ROS). Finally, by using real time quantitative polymerase chain reaction (RT-qPCR), the expression of CDK2 and Survivin in drug-treated HeLa cells were investigated to explore the PDT action of ADCPPa.

Materials and methods

General remarks

Chlorophyll paste was bought from Shandong Guangtongbao Pharmaceuticals Co., Ltd (Qingzhou city, Shandong,

Scheme 1 Synthesis of ADCPPa: **a** 30% HBr (in acetic acid); **b** LiOH, 4-methylmorpholine-N-oxide, tetrapropylammonium perruthenate; **c** dicyanomethane, triethylamine



China). SA and DM were bought from Sinopharm Chemical Reagent Co. Ltd (Shanghai, China). Dulbecco's modified eagle medium, penicillin, fetal bovine serum (FBS), and streptomycin were purchased from Beijing Dingguo Biotechnology Co (Beijing, China). Dimethyl sulfoxide and 3-(4,5-dimethylthiazol-2-yl)-2,5-diphenyltetrazolium bromide were purchased from Sigma (Shanghai, China). Phosphate buffered saline purchased from Invitrogen (Beijing, China). Phosphate-buffered saline (PBS) used was prepared by mixing stock solutions of NaH_2PO_4 and Na_2HPO_4 . RNAPure Tissue Kit (DNase I) and PrimeScript™ 1st strand cDNA Synthesis Kit were bought from Tiangen Biotech (Beijing) Co. Ltd; SYBR® Premix Ex Taq™ (Tli RNaseH Plus) was bought from TAKARA Biotechnology (DaLian) Co., Ltd.

All the chemical reactions were performed away from sunshine under nitrogen atmosphere. $^1\text{H-NMR}$ (400 MHz) and $^{13}\text{C-NMR}$ spectra (100 MHz) were recorded on an AMX400 spectrometer (Bruker, Bremen, Germany) with tetramethylsilane as an internal standard. Mass spectra were recorded with a Hitachi VG-7070 spectrometer. UV–Vis absorption in methanol (2.15×10^{-5} M) in the 300–800 nm range were recorded using LAMBDA 25 spectrometer (PerkinElmer). The emission spectra were recorded using spectrofluoro-photometer with a 150 W xenon lamp as a visible excitation light source (RF-5301PC, Shimadzu). All spectra were obtained in a quartz cuvette (path length = 1 cm). The excitation and emission slit widths were both 10 nm, and photomultiplier tube voltage of 700 V.

Synthesis of 3-(1-hydroxyethyl)-3-devinylmethylpyrophephorbide-a (HMPPa)

According to the literature (Zhang et al. 2016), MPPa (78 mg, 0.14 mmol) was dissolved in 10 mL of 33% hydrobromic acid–ethanol solution, and stirred for 5 h at 50 °C. The reaction mixture was then concentrated under vacuum condition to remove the solvent. Then 30 mL of water was added and the mixture was extracted with 30 mL dichloromethane for three times. The organic layer was washed by saturated sodium chloride solution, dried by anhydrous Na_2SO_4 , and concentrated to remove the solvent. The product was purified by gel column chromatography separation with ethyl acetate/methanol (5:1) to give a bluish-green solid (60%).

HMPPa

UV–Vis(CH_3OH) λ_{max} : 405, 502, 542, 601, 664; $^1\text{H NMR}$ (CDCl_3) δ : -1.91(s, 1H, NH), -0.12 (s, 1H, NH), 1.67 (t, J = 7.6 Hz, 8- CH_3), 1.76 (d, J = 8.4 Hz, 3H, 18- CH_3), 2.11 (d, J = 6.4 Hz, 3H, 3 2 - CH_3), 2.21–2.26 (m, 2H, 17 1 - CH_2), 2.60–2.71 (m, 2H, 17 2 - CH_2), 3.21 (s, 3H, 7- CH_3), 3.37

(s, 3H, 2- CH_3), 3.38 (s, 3H, 12- CH_3), 3.58 (s, 3H, 17- OCH_3), 3.61–3.68 (m, 8- CH_2), 4.18–4.23 (m, 1H, 17-CH), 4.23–4.44 (m, 1H, 18-CH), 5.06 (d, J = 17.2 Hz, 1H, 13 2 - CH_2), 5.26 (d, J = 19.6 Hz, 1H, 13 2 - CH_2), 6.31–6.39 (m, 1H, 3 1 -CH), 8.49 (s, 1H, 20-H), 9.34 (s, 1H, 10-H), 9.61(s, 1H, 5-H).

Synthesis of 3-acetyl-3-devinylpyrophephorbide-a (APPa)

HMPPa (28 mg, 0.05 mmol) was dissolved into 20 mL of 25% methanol–water solution. Add 5 mL of 2 M LiOH aqueous solution into the above mixture, which was then stirred for 2 h under reflux conditions. After cooling, adjust the pH value of the reaction mixture to 5 with 2 M HCl aq. Then extract with 60 mL dichloromethane for three times. The organic layer was dried and concentrated to remove the solvent. The residue was dissolved in 4 mL dried dichloromethane, and 4-methylmorpholine N-oxide (5 mg) was then added. The mixture was stirred for 30 min, then add tetrapropylammonium perruthenate in batches (11 mg). After stirring for 3 h at r.t., 30 mL water was added. The organic layer was dried by anhydrous Na_2SO_4 and then concentrated. The residue was purified by gel column chromatography separation with benzene/acetone (8:1) to give a brownish-green solid (80%).

APPa

UV–Vis (CH_3OH) λ_{max} : 414, 513, 548, 623, 683; $^1\text{H-NMR}$ (CDCl_3): -2.07 (s, 1H, NH), -0.11 (s, 1H, NH), 1.69 (t, J = 7.8 Hz, 8- CH_3), 1.78 (d, J = 7.2 Hz, 3H, 18- CH_3), 2.20–2.25 (m, 2H, 17 1 - CH_2), 2.59–2.77 (m, 2H, 17 2 - CH_2), 3.20 (s, 3H, 3 1 - CH_3), 3.26 (s, 3H, 1- CH_3), 3.60–3.68 (m, 8H, 7- CH_3 , 12- CH_3 , 8- CH_2), 4.34–4.36 (m, 1H, 17-CH), 4.53–4.57 (m, 1H, 18-CH), 5.08 (d, J = 19.6 Hz, 1H, 13 2 - CH_2), 5.26 (d, J = 19.6 Hz, 1H, 13 2 - CH_2), 8.77 (s, 1H, 20-H), 9.49 (s, 1H, 10-H), 9.93 (s, 1H, 5-H); $^{13}\text{C NMR}$ (CDCl_3): 11.1, 12.0, 13.2, 17.3, 19.4, 23.3, 29.3, 31.0, 33.4, 48.1, 49.2, 51.6, 94.3, 100.2, 103.5, 106.7, 129.5, 131.3, 134.1, 135.3, 137.3, 138.9, 139.1, 144.8, 148.7, 151.8, 154.9, 161.3, 170.1, 173.3, 195.9, 199.2, 206.7; FAB-MS: 550 (M^+); anal calcd for $\text{C}_{33}\text{H}_{34}\text{N}_4\text{O}_4$: C, 71.98; H, 6.22; N, 10.17; found C, 72.11; H, 6.30; N, 10.03;

Synthesis of the title compound ADCPPa

Dissolve APPa (25 mg, 0.05 mmol) in a mixture of ethanol (2 mL) and dichloromethane (4 mL), then add dicyanomethane (110 mg, 1.65 mmol) and triethylamine (0.2 mL) into the mixtures, which were stirred for 3 h at 85 °C. After the reaction mixtures were cooled, pour them into 30 mL water, and extract with 25 mL dichloromethane for three times. The organic layer was dried by anhydrous Na_2SO_4

and concentrated. The residue was separated by gel column chromatography with benzene/acetone (10:1) to give a dark green solid (60%).

ADCPPa

UV–Vis (CH₃OH) λ_{\max} : 403, 534, 570, 654, 713; ¹H-NMR (CDCl₃): 1.55–1.59 (t, $J = 7.8$ Hz, 8-CH₃), 1.77 (d, $J = 7.2$ Hz, 3H, 18-CH₃), 2.05–2.13 (m, 2H, 17¹-CH₂), 2.20–2.26 (m, 2H, 17²-CH₂), 2.86 (s, 3H, 3¹-CH₃), 3.00 (s, 3H, 7-CH₃), 3.10 (s, 3H, 2-CH₃), 3.24 (s, 12H, 2-CH₃), 3.39–3.45 (m, 2H, 8¹-CH₂), 4.04–4.06 (m, 1H, 17-CH), 4.23–4.27 (m, 1H, 18-CH), 5.10–5.27 (dd, $J = 20.8$ Hz, 2H, 15¹-CH₂), 8.20 (s, 1H, 20-H), 8.68 (s, 1H, 10-H), 9.05 (s, 1H, 5-H); ¹³C NMR(CDCl₃): 11.1, 12.0, 13.2, 17.3, 19.4, 23.3, 29.3, 31.0, 33.4, 48.1, 49.2, 51.6, 94.3, 100.2, 103.5, 105.0, 110.0, 116.0, 116.4, 106.7, 129.5, 131.3, 134.1, 135.3, 137.3, 138.9, 139.1, 144.8, 148.7, 151.8, 154.9, 161.3, 170.1, 173.3, 195.9, 199.2, 206.7; FAB-MS: 598 (M⁺); anal calcd for C₃₆H₃₄N₆O₃: C, 72.22; H, 5.72; N, 14.04; found C, 72.16; H, 5.88; N, 13.94.

Cell culture and in vitro cytotoxicity

The human cervical cancer cell line (HeLa) was cultured in Dulbecco's modified Eagle's medium (DMEM, Gibco) supplemented with 10%(v/v) FBS and 1% antibiotic (100 µg/mL penicillin–100 µg/mL streptomycin, Life Technologies, USA) in an incubator (5% CO₂, 98% humidity, 37 °C). The cytotoxicity was investigated by methylthiazolyldiphenyl-tetrazolium bromide (MTT) assay. HeLa cells were divided into experimental group (ADCPPa group, L+) treated with different concentrations of ADCPPa and exposed to light, and control group (blank group, L-) treated with drugs without light.

Precisely, HeLa cells were seeded in a 96-well plate with an initial density of 1×10^4 cells per well and incubated for 24 h (37 °C, 5% CO₂). Then HeLa cells in the experimental groups and the control groups were treated with different concentrations of ADCPPa (2.5, 5, 10, 15, 20, 25 and 30 µg/mL, respectively). Then the cells in the experimental groups were incubated for 4 h followed by exposure to visible light for 10 min, and then cultured in dark for additional 24 h in DMEM as described above, while the control group was incubated for the same time without light. Then MTT dyes (100 µL, 0.5 mg/mL) were added to the wells, and incubated for another 4 h. Remove the MTT solutions and dissolve the formazan crystals with 100 µL of DMSO. Finally, the absorbance of each probe was read on a microplate reader at 490 nm. Cell viability (%) was calculated according to the following equation:

$$\text{Cell viability (\%)} = A_{(\text{sample})} / A_{(\text{control})} \times 100\%$$

where $A_{(\text{sample})}$ represents A values of the wells treated with ADCPPa, and $A_{(\text{control})}$ represents those of the wells treated with DMEM + 10% FBS.

Cellular uptake test

Drug uptaking behavior in HeLa cancer was performed by Leica DM IL LED fluorescent inverted microscope (FIM). HeLa cells were incubated for 24 h. After discarding the medium, cells were rinsed with PBS and treated with 20 µg/mL ADCPPa for 15, 30, 45, 60 and 180 min, respectively. Then, glutaraldehyde solution (1 mL, 2.5%) was used to fix the cells (10 min, 37 °C). Then the glutaraldehyde solution was removed and the cells were rinsed extensively with PBS, subsequently stained with 1 mL of 1 µg/mL DAPI probe for 10 min

Morphological changes of HeLa cells after PDT

Morphological changes of HeLa cells after treatment of ADCPPa were also analyzed by FIM. HeLa cells were incubated for 24 h, the medium was then removed. The cells were rinsed with PBS, and treated with 20 µg/mL ADCPPa for 4 h, followed by exposure to infrared light (675–780 nm, 10 min, 10 J/cm²). The morphological changes were observed after 1, 3, 6, 12 and 24 h, respectively, comparing with the cells without light treatment.

Photochemical mechanism of ADCPPa in PDT

SA and DM could selectively quench oxygen-free radicals and singlet oxygen (¹O₂), respectively, making them inoperative. In this section, the cells were divided into three groups: (1) L+ groups: treated with different concentrations of ADCPPa and exposed to light; (2) SA groups: treated with ADCPPa and SA (20 mmol/L), and exposed to light; (3) DM groups: treated with ADCPPa and DM (40 mmol/L), and exposed to light. Precisely, HeLa cells were incubated in DMEM 24 h as described above. Hundred microliters of different concentrations of sample (2.5, 5, 10, 15, 20, 25 and 30 µg/mL) were added to each well of L+ group, SA groups and DM groups. To SA groups was added 20 µL SA and to DM groups was added 40 µL DM. Then incubated for 4 h followed by exposure to light for 10 min. Cell viability was determined as previously mentioned.

Singlet oxygen quantum yield

In this paper, diphenylisobenzofuran (DPBF) was used as a ¹O₂ trapping reagent. Typically, 3 mL of a stock solution of DPBF in DMF (60 µM) was added 50 µL ADCPPa solution (2.8 µM), then the mixture was placed in a sealed quartz cuvette. A 5 mW Nd:YAG laser (675–780 nm) was used as

the light source to excite the sensitizer. The absorbance of the solution at 415 nm was measured every 10 s for a 120 s period with UV–Vis spectrophotometer. The decrease of the absorbance resulted from DPBF was measured and corrected. The Singlet oxygen ($^1\text{O}_2$) quantum yield (Φ_Δ) of ADCPPa is calculated using the following formula (Zimcik et al. 2007):

$$\Phi_\Delta(S) = \Phi_\Delta(R)k^S I_{aT}(R)/k^R I_{aT}(S) \quad (1)$$

$$I_a = I_0(1 - e^{-2.3A}). \quad (2)$$

Superscript *S* and *R* indicate the sample and DPBF, respectively. I_a is the total amount absorbed light of the PS. *A* is the absorbance at irradiation wavelength. A_0 and A_t are the absorbances of the DPBF at 415 nm before irradiation and after irradiation time *t*, respectively, and *k* is a slope of a plot of the dependence of $\ln(A_0/A_t)$ on irradiation time *t*. The $^1\text{O}_2$ yield during the photochemical process was obtained by a first-order linear least-squares model using the natural logarithm values of DPBF absorption at 415 nm plotted against the irradiation time. The $^1\text{O}_2$ yield of ADCPPa was calculated with methylene blue (MB) as a standard. The slope for MB and ADCPPa was obtained after fitting with a linear function.

Fluorescence quantitative polymerase chain reaction (PCR)

HeLa cells in logarithmic growth phase were seeded in a six-well plate with an initial density of 1.5×10^5 cells per well and incubated for 24 h (37 °C, 5% CO_2). Then ADCPPa (30 $\mu\text{g}/\text{mL}$) was added per well and incubated for 4 h and then exposed to light for 10 min. Then the cells cultured with different time (0, 6, 12, 24 h) were collected for later use. The total RNA extraction and cDNA synthesis was performed in the usual way according to the literatures (Ramalho et al. 2004; Williams et al. 1992). The reverse transcription (RT) reaction was carried out at 42 °C for 45 min, then RNase inhibitors were inactivated at 95 °C for 5 min. The fluorescence quantitative PCR was performed by SYBR[®] Premix Ex Taq[™] (Tli RNaseH Plus) according to the instruction using gene-specific primers and the internal control GADPH primers. Precisely, 2 μL of cDNA solution was added to 20 μL of PCR mixture (SYBRPremix Ex Taq (Tli RNaseH Plus) containing 10 μM each primer (Forward primer and Reverse Primer) and ROX Reference Dye (50 \times) for specific amplification as the follows: 40 cycles of denaturation (95 °C for 30 s), primer annealing (56 °C for 30 s), and extension (72 °C for 1 min). PCR products were analyzed by electrophoresis in 1.5% agarose gel.

Results and discussions

Synthesis and spectral properties

The inhomogeneous electric charge distribution of the multi- π aromatic system caused by the asymmetrical chemical structure of MPPa lets it have many active sites in periphery. The exocyclic nonaromatic unsaturated substituents, such as carbonyl or vinyl group are not involved in the conjugation of multi- π aromatic system (Ivanov and Boldyrev 2014), possessing the typical chemical characteristics of carbonyl or vinyl group, based on which structural modifications of MPPa are moderately feasible. The Qy peak of MPPa in UV–Vis spectrum was at 667 nm. In order to redshift the Qy peak (long wavelength absorption) and to improve penetration depths, strong electron-withdrawing group dicyanomethylene moiety was introduced on the 13¹-position to expand the conjugation system of the macrocycle. Scheme 1 shows the synthesis process of ADCPPa. At first, the vinyl group at C-3 was converted into hydroxyl group through electrophilic addition reaction in hot HBr-acetic acid solution, meanwhile the ester group at C-17 was hydrolyzed into carboxylic group. The obtained intermediate HMPPa was oxidized by tetrapropyl ammonium perruthenate to obtain the APPa, which reacted with dicyanomethane under alkaline conditions to give the target compound ADCPPa. As expected, the introduction of dicyanomethylene moiety brought about obvious red shift of its long wavelength absorption, showing Qy peak at 713 nm, with a 46 nm red-shift comparing with MPPa (667 nm) (Fig. 2) Moreover, ADCPPa showed excellent fluorescence characteristics, displaying a fluorescence emission peak at near-infrared 723 nm under the excitation of 449 nm, which means that the title compound has the prospects for targeting fluorescence imaging in tumor diagnosis, because the red fluorescence emitted by ADCPPa under light makes the target cells more palpable (Silva et al. 2013).

Photobleaching of ADCPPa

The photobleaching is an important property of a PS, and it is a common phenomenon during PDT. Generally, PS will interact with light to generate ROS, and can be reused or recycled during PDT without being consumed. However, during the same period, PS will suffer from serious of photochemical reaction process, such as photodecomposition, photoionization, photoassociation, photoisomerization or photo-oxidation/reduction, all of which will consume the PS and cause the structural change of PS, leading to a decrease of PDT effect (Yu et al. 2001). This is known as photobleaching. Due to the negative effect of photobleaching to PDT effect, it is necessary to determine to the photobleaching rate of PS. For the irradiation wavelength

Fig. 2 The absorption and fluorescence spectrum of ADCPPa in CH₃OH

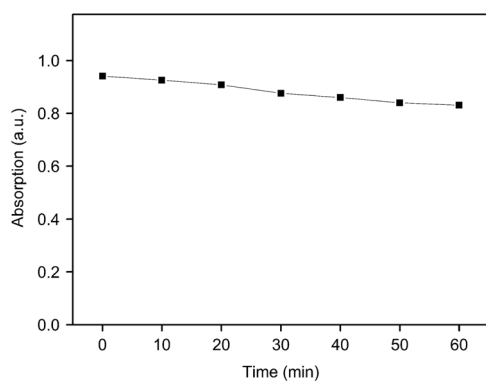
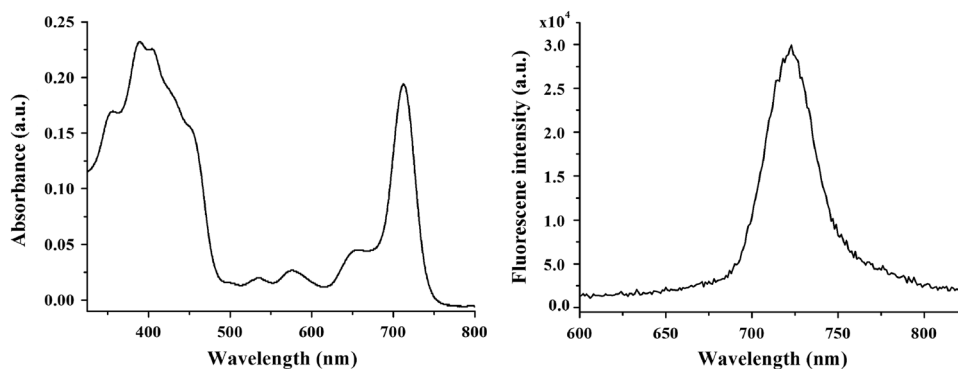


Fig. 3 Time dependence of the intensities of absorption maxima at 681 nm (20 °C, 20 μM) in PBS

used to excite the sensitizers was about 675–780 nm from a Nd:YAG laser (675–780 nm), we here determine the time dependence of the intensities of absorption maxima at 681 nm (20 °C, 20 μM) in PBS. The data on the time dependence of absorption maxima is summarized in Fig. 3. At 20 °C, the photobleaching of band at 681 nm shows a gentle and flat manner. Especially, at the stage of illumination time less than 10 min, the decrease of intensity of absorption maxima is approximately 1.6%, not significant. Even though after extending the illumination time to 60 min, the decrease of intensity of absorption maxima is about 9%. As mentioned earlier, the PS could achieve good PDT effect after being exposed to light for 10 min, therefore the photobleaching has a little influence on PDT effect of ADCPPa.

Cellular uptake

PSs should be able to enter the cells before taking effect, hence PDT drugs need to be lipophilic to pass through biomembranes, and reach subcellular sites for further oxidative damage and subsequent cell-destroying (Bonnett and Martínez 2002). Generally, PSs travel intravenously as complexes of serum proteins (Wang et al. 2011) and are taken up preferentially by rapidly proliferating tissue, such as tumor tissue (Allison et al. 2008; Nowis et al. 2005), then

it was activated by an appropriate wavelength of light in the presence of oxygen, producing ROS, which start a cascade of molecular and biochemical events resulting in cell death via apoptotic or necrotic mechanisms (Mroz et al. 2011; Buytaert et al. 2007). Hence, prior the cytotoxicity research, a research on the interaction of PS with plasma membrane for cellular uptake is needed. Most of the porphyrin PSs are localized in mitochondria and cell nucleus. In the present uptake test, the nucleus was firstly stained by a DAPI dye solution, after which the nucleus can be easily observed due to the blue fluorescence. If the PS could be uptaken successfully by cells, the corresponding red fluorescent emitted from PS (such as ADCPPa) would make the cells palpable. In the experimental group, the cells were incubated with 20 μg/mL ADCPPa for 15, 30, 45, 60 and 180 min, respectively. Then cell imaging was observed on a FIM.

As shown in Fig. 4, the cells in control group without DAPI dye and light showed gray white without any changes over the time, while in the experiment group after treatment with ADCPPa and light, the cell nucleus showed obvious *blue fluorescence*, and the brightness was increasing. After incubation with ADCPPa for 15 min, weak red fluorescence was observed from many of the cells, suggesting that the PS began to enter the cells. After 30 min incubation, the brightness of red fluorescence enhanced significantly, and the signal intensity was stronger than that observed at 15 min. After incubation for 1 h, the red fluorescent signal can be detected from almost all cells, and the signal intensity was stronger. Longer incubation showed minor change, suggesting that cell uptake has reached a point of saturation. The above analysis has proved that ADCPPa can be successfully and quickly uptaken by Hela cells, implying that the PS could take effect more quickly in practical application.

Photodynamic activities

A high photocytotoxicity within the aerobic tissues and low dark toxicity are important for PS. In this part, Hela cells

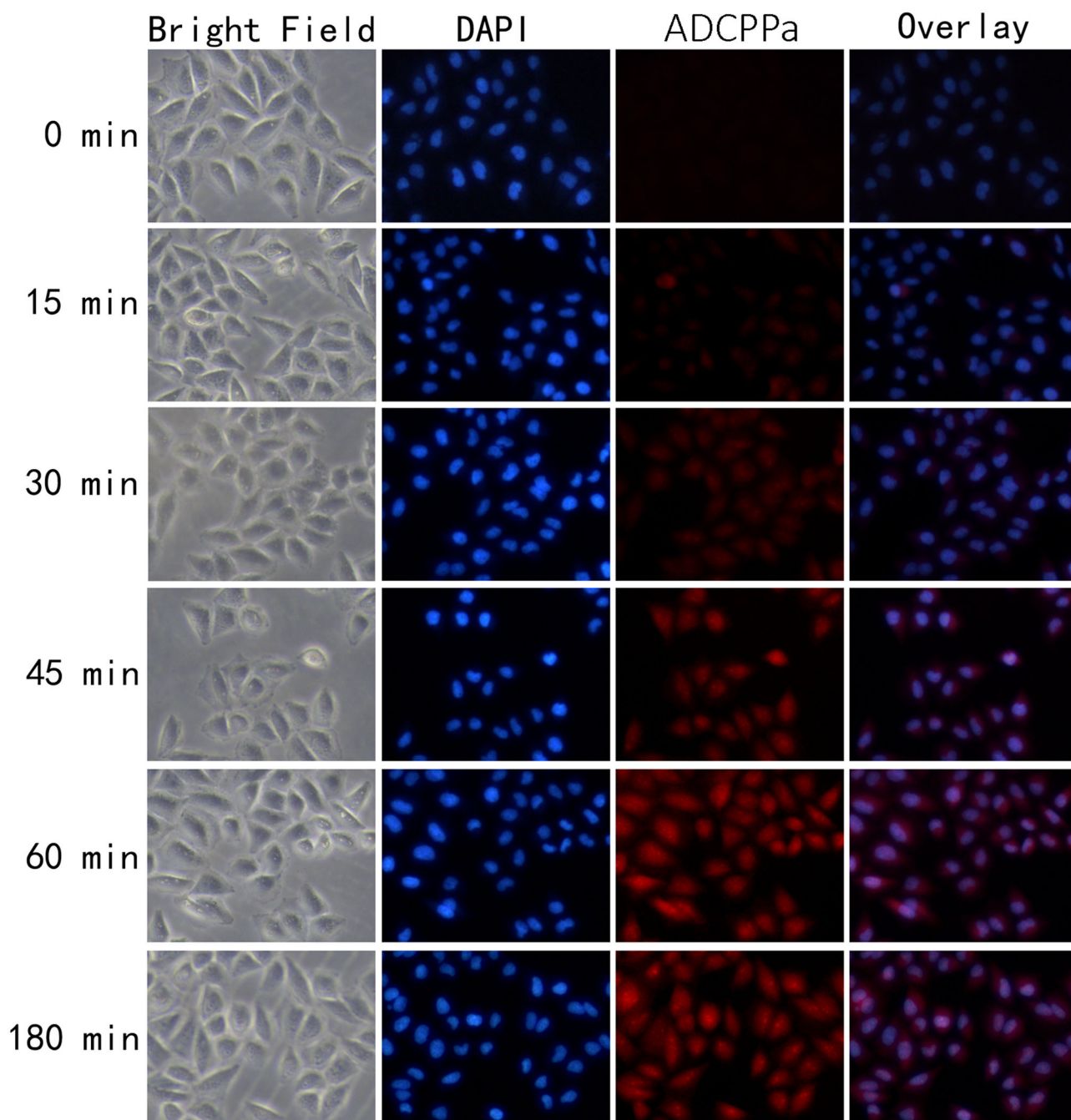


Fig. 4 Fluorescence-inverted microscopic images of cellular uptake test: HeLa cells were incubated with ADCPPa (1 mL, 20 $\mu\text{g}/\text{mL}$) at 37 $^{\circ}\text{C}$ for 15, 30, 45, 60 and 180 min, respectively. The nucleus was

stained with DAPI (blue), the red fluorescence was due to ADCPPa (color figure online)

were used to detect the anticancer activity of our designed compound. The viability of HeLa cells incubated with different concentrations of ADCPPa and Mppa were analyzed by MTT assay. The HeLa cells were divided into the experimental group (ADCPPa group) and control group (blank group). The experimental groups were treated with different concentrations of ADCPPa (2.5, 5, 10, 15, 20, 25 and 30 $\mu\text{g}/\text{mL}$, respectively) and exposed to light; the

control groups were treated with drugs and not exposed to light.

Figure 5 shows the photodynamic activity of the ADCPPa against HeLa cells. *Black columns* stand for the cell viability of ADCPPa experiment groups, *red columns* stand for the cell viability without light. The control groups (*red columns*) treated with different concentrations of ADCPPa without light show high cell viability (>85%),

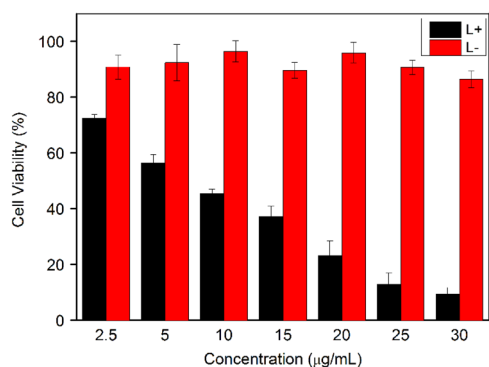


Fig. 5 The photo cytotoxicity and dark toxicity of ADCPPa against HeLa cells. The *black columns* stand by the experimental groups, and the *red columns* stand for the control groups (color figure online)

suggesting that ADCPPa caused low dark toxicity in the present study. The experimental group test showed that with the increasing concentrations of drugs, the cell viability rate declined obviously. That's to say, cell survival incubated with ADCPPa with red-light irradiation was related to the ADCPPa concentration, suggesting the inhibition ability of ADCPPa was concentration-dependent. When the concentration of ADCPPa reached to 30 µg/mL, the cell viability lowered to 7%, suggesting that the ADCPPa had strong photodynamic effects on the HeLa cell at such concentration under light (713 nm, 10 J/cm²). The IC₅₀ of ADCPPa against cancer cells was 6.21 µg/mL. Moreover, as investigated in our previous study (Li et al. 2016), the MPPa also showed antitumor activity with a cell viability of 55% at the concentration of 5 µM (27 µg/mL), yet the present compound led to a cell viability of 13% at the concentration of 25 µg/mL, showing a much better activity compared with the leading compound.

Mechanism of photochemical processes in PDT

After a PS is administered to the body and exposed to light for some time (drug-to-light interval), the inactive drug is electronically excited after irradiated and carries on a type I reaction to form superoxide anion and radicals, or performs a type II reaction to form singlet oxygen (¹O₂) (Fig. 1). Both of the ROS can cause cell death, yet the ¹O₂ generated through type II reaction is considered for the major lethal material. To investigate the mechanism of photochemical processes in PDT, SA and DM were utilized in our research. SA and DM could selectively react with oxygen free radicals and singlet oxygen respectively, making the corresponding ROS invalid on cancer cells (Li et al. 2016; Sparrow et al. 2003). HeLa cells in our experiments were divided into three groups: (1) L+ groups: treated with different concentrations of ADCPPa exposed to light; (2) SA groups: treated with ADCPPa and SA (20 mmol/L), and

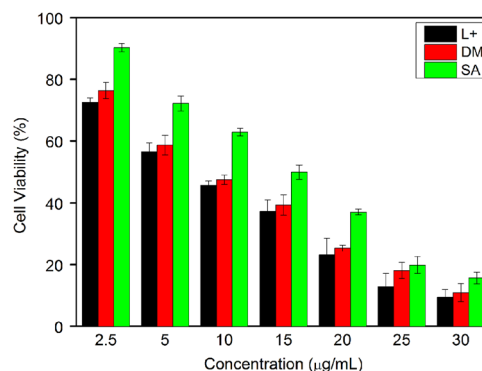


Fig. 6 Cell viability of three different PDT processing methods. L+ stands for the groups treated with ADCPPa under light. DM stands for the groups treated with ADCPPa and D-mannitol under light; SA stands for the groups treated with ADCPPa and sodium azide under light

exposed to light; (3) DM groups: treated with ADCPPa and DM (40 mmol/L), and exposed to light.

Figure 6 show the influences of three different PDT processing methods on cytotoxicity effects. The cell viability of SA groups was much higher than that of DM group at various concentrations, especially at high concentrations (40 µg/mL), suggesting that the key ROS (singlet oxygen) have been quenched, resulting in low cytotoxicity to HeLa cells, therefore Type II reaction played a prominent role in vitro. Moreover, the cell viability of DM groups were also slightly higher than that of L+ group, suggesting that Type I photodynamic reactions also occupied a certain proportion during PDT, but not essentially. Generally, Type II reaction would take place in the presence of tissue oxygen, yet in the present cell experiments, the cancer cells may also provide some integral substrate for PS to complete the Type I reaction, hence coexistence of Type I and Type II was rational.

Singlet oxygen quantum yield of ADCPPa

As mentioned earlier, production of singlet oxygen (¹O₂) is based on the energy transfer from the triplet state of PSs to ground state molecular oxygen and it has been demonstrated that generation of ¹O₂ is responsible for the initiation of cell death (Ashikaga et al. 2000). The above research has disclosed that the generation of singlet oxygen plays a major role in photochemical process of ADCPPa, therefore the determination of singlet oxygen quantum yield of ADCPPa is indispensable for mechanistic investigation and PS development. In this study, the methods employed are based on the reaction of ¹O₂ with a singlet oxygen quencher and the time-dependent spectrofluorimetric determination of quencher concentration (Berneburg et al. 1999). 1,3-diphenylisobenzofuran (DPBF) has been reported as a good candidate for ¹O₂ detecting probe (Belfield et al. 2005), its

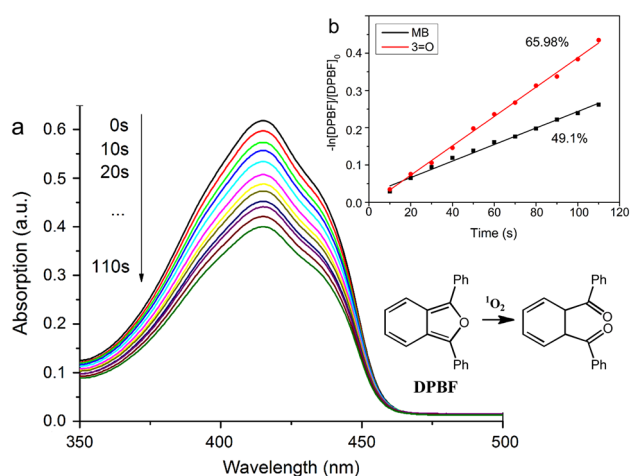


Fig. 7 **a** Photodecomposition of DPBF by $^1\text{O}_2$ after irradiation of ADCPPa in DMF (monitoring the maximum absorption of DPBF at 415 nm). **b** The linear fitting curve comparison of ADCPPa and methylene blue

conjugated structure can be destroyed after reacting with singlet oxygen, which can be detected by spectrofluorimeter. The decay of the absorption of DPBF at 415 nm corresponds to the ability of ADCPPa to produce singlet oxygen. The changes in intensity of the emission peak reflects the singlet oxygen production generation. Both the of DPBF and ADCPPa solutions have fluorescence emission peak at 415 nm.

The $^1\text{O}_2$ yield during the photochemical process was obtained by a first-order linear least-squares model using the natural logarithm values of DPBF absorption at 415 nm plotted against the irradiation time. As shown in Fig. 7a, the absorption at 415 nm significantly decreased over the time. The $^1\text{O}_2$ quantum yield of ADCPPa in DMF was calculated using MB as a standard, whose singlet oxygen quantum yield (Φ_Δ) in DMF is 49.1%. The slope for ADCPPa and MB was obtained after fitting with a linear function ($R^2 \hat{=} 0.99752$). The singlet oxygen quantum yield (Φ_Δ) of ADCPPa in DMF is 65.98% (Fig. 7b), suggesting the title compound has remarkable capacity to generate singlet oxygen during the photochemical process. However, the singlet oxygen yield of PPa is only about 39.2% as reported in our previous paper (Cheng et al. 2017), which has partially explained why ADCPPa could efficiently inhibit the growth of cancer cell in PDT experiments than the leading compound.

Morphological changes of HeLa cells after PDT

The in vitro PDT test mentioned earlier showed that ADCPPa possessed strong inhibition ability against tumor growth. We here tried to visually examine the tumor cell phenotype after treatment of ADCPPa by FIM. The cell phenotype was analyzed after incubation with ADCPPa

(20 $\mu\text{g}/\text{mL}$) and exposing with light (713 nm, 10 J/cm^2) for 3, 6, 9, 12, 24 h, respectively, compared with the cancer cells without any treatment.

As shown in Fig. 8a, normal HeLa cells are spindle-shaped with steady cytoplasm. After treatment with PDT for additional 3 h (Fig. 8c), the cells become rounder, and shading degree decreases obviously. After 6 h (Fig. 7d), dilation of intercellular space and injury of the membrane were observed, meanwhile the cell adhesive ability decreased. After prolonged incubation (Fig. 8e, f), the entire membrane structure of the cells was destroyed and almost all the cells died, emerging sporadically apoptotic body. Morphological changes of HeLa cells clearly showed that ADCPPa could cause cellular damage under light. Although PDT can induce cell death by several mechanisms, including apoptosis, necrosis, mitotic catastrophe, and autophagy, yet the mechanism of cell death caused by PS was not single and immutable (Dewaele et al. 2010).

Preliminary antitumor action research of ADCPPa

The mechanism of the PDT-mediated cytotoxic effect is still not fully understood. It was reported that PDT-induced oxidative stress could increase the expression of early response genes, the cellular stress protein and heme oxygenase (Luna et al. 1994). Moreover, it is widely acknowledged that cell cycle arrest is an important cause of cell apoptosis. Many porphyrin derivatives, such as protoporphyrin IX (Li et al. 2013), gold (III) porphyrin complexes (Tu et al. 2009), TMPyP4 (Shammas et al. 2003), were reported to be able to induce cell cycle arrest in cancer cells. Generally, cyclin-dependent kinases (CDKs) and cyclin are the core factors of endogenous regulation and control of cell cycle, especially CDK2, playing an important role in tumor cells proliferation (Malumbres and Barbacid 2009). The reduction in CDK2-related expressed genes would lead to cell cycle arrest at G0–G1 phase, consequently the DNA synthesis and cell proliferation would be inhibited, therefore determination of the CDK2 expression is an effective way to study the influence of drugs on cancer cells. If CDK2 expression is upgraded in drug-treated cancer cells, it may be presumed that the PS can effectively induce cell apoptosis. Moreover, Survivin, which exhibits divergent functions such as regulating cell proliferation and cell death, is the strongest inhibitor of apoptosis that has been found among inhibitor of apoptosis protein family. (Garg et al. 2016). Generally, Survivin is specially expressed in embryonic cells and tumor cells, but is seldom expressed in normal adult cells. Over-expression of Survivin inhibits both intrinsic and extrinsic pathways of apoptosis. (Altieri 2001) Survivin expression in tumor cells may promote tumor progression by various pathways, i.e., dysregulation of apoptosis and cell division, therefore, if obvious change in expression of Survivin is

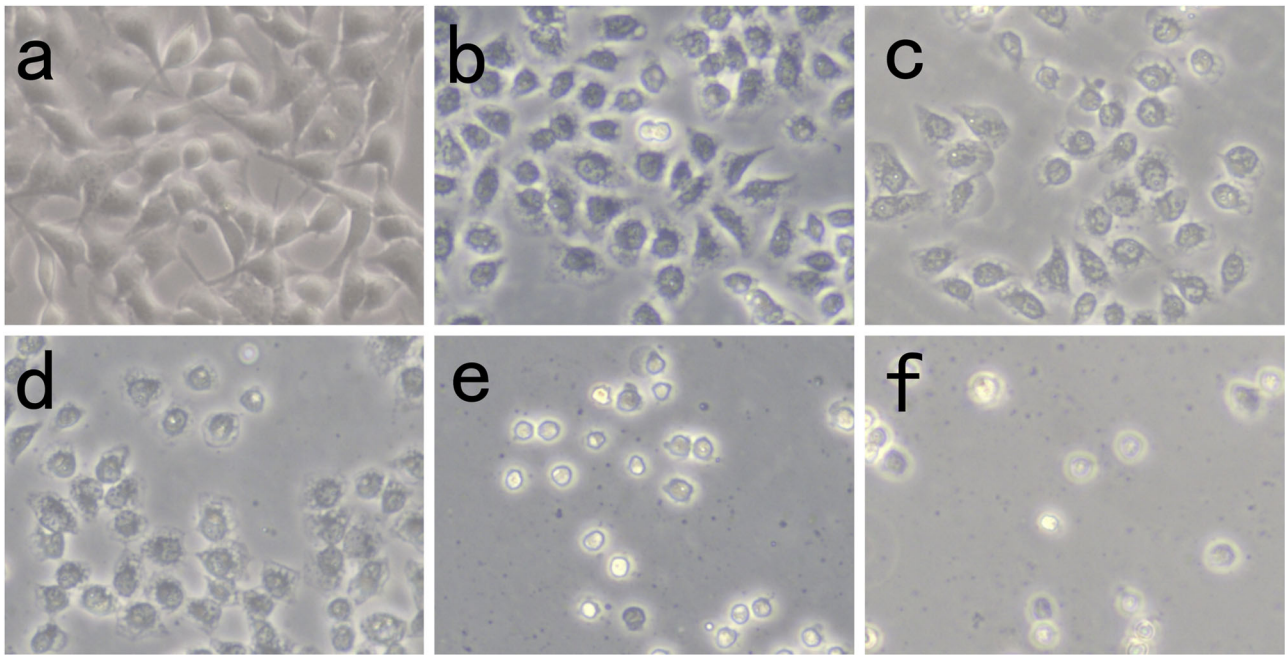
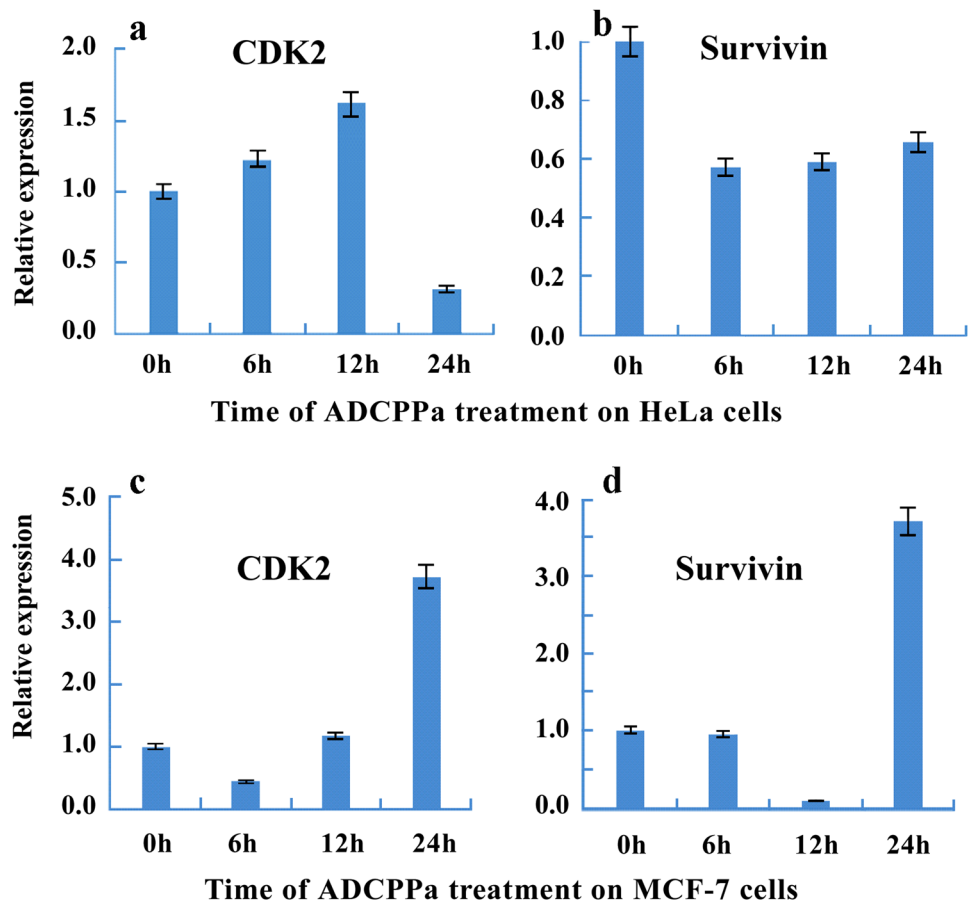


Fig. 8 Morphological changes of HeLa cells incubated with 20 µg/mL ADCPPa under light: **a** 0 h; **b** 1 h; **c** 3 h; **d** 6 h; **e** 12 h; **f** 24 h

Fig. 9 The relative expressions under ADCPPa treatment: **a** CDK2 in HeLa cells; **b** Survivin in HeLa cells; **c** CDK2 in MCF-7 cells; **d** Survivin in MCF-7 cells



found in PS-treated cancer cells, it can be concluded that the PS can influence the expression of Survivin, subsequently resulting the cell death.

Therefore, in this paper, by using qRT-PCR, we tried to investigate the expression CDK2 and Survivin in drug-treated HeLa cells and MCF-7 cells to explore the

PDT action of ADCPPa. Figure 9a, b shows the expression of CDK2 and Survivin in HeLa cells treated with ADCPPa. It can be seen that after treatment with ADCPPa, the expression of CDK2 increased gradually over the time, and peaked after 12 h, about 1.6 times as high as that of the control group (Fig. 9a). After 24 h treatment, expression of CDK2 was lower than that of the control group, about 0.3 times, which suggested that the expression of CDK2 was significantly inhibited by ADCPPa at this time, leading to cell cycle arrest and programmed cell death. In case of Survivin (Fig. 9b), the expression of Survivin in ADCPPa-treated HeLa cells showed an downward trend first, but then increased over the time, however, the expressions were apparently less than that of the control, about 0.57, 0.59 and 0.66 times at 6 h, 12, 24, respectively, suggesting our compound could degrade the expression of Survivin, displaying a negative regulatory effect. As mentioned earlier, Survivin expression in tumor cells may promote tumor progression, the negative regulation by ADCPPa would undoubtedly impel cell death.

Moreover, we have also investigate the expression regulating effect on breast cancer MCF-7 cells to see if the PS has an effect on the expression regulating of other cells. As shown in Fig. 9c, the expression of CDK2 in MCF-7 cells treated with ADCPPa decreases first, then increases gradually over the time. The lowest expression level is at 6 h, about 0.4 times as high as that of the control group. With the passage of time the expression level rise rapidly, reaching 3.7 times the size of control group, which suggested ADCPPa would take effect after 6 h treatment. The generous gene CDK2 expression at 24 h was supposed to be a sort of cellular stress response to external stimulus. For Survivin (Fig. 9d), the expression in MCF-7 cells treated with ADCPPa decreases first, reaching the minimal level after 12 h, about 0.1 time as high as that of control. However, after 24 h, the expression level rise rapidly, reaching 3.7 times the size of control group, which was also considered as a sort of cellular stress response, leading an obvious rebound of expression. All in all, the target compound has important regulating effect on expression of CDK2 and Survivin. It can inhibit the HeLa cell cycle and induce apoptosis and kill the tumor cells thoroughly.

Conclusions

In summary, ADCPPa has many properties which make it a promising PS for PDT and photodiagnosis. It is endowed with maximal absorption wavelength at 713 nm, red fluorescence at 723 nm after 449 irradiation, high singlet oxygen quantum yield (65.98%), and excellent anti-photobleaching

ability. In vitro PDT study has shown that ADCPPa had strong photodynamic effects and low dark toxicity against the cancer cells. Cell uptaking test indicated ADCPPa could quickly enter the cells in less than 1 h, suggesting that the PS could take effect more quickly in practical application, which also improved the feasibility in clinical application. In addition, qRT-PCR has showed that the target compound has important regulating effect on expression of CDK2 and Survivin. All in all, our results indicated that ADCPPa was an effective PS as a new drug candidate in PDT and was worth for further study.

Acknowledgements Financial support of this research was provided by National Natural Science Foundation of China (No. 20972036, 21272048, 21471041), the Natural Science Foundation of Heilongjiang Province (No.B20913), the Program for Scientific Technological Innovation Team Construction in the Universities of Heilongjiang Province (No. 211TD010), the Scientific Research Fund of Heilongjiang Provincial Education Department (No.12531194), the Natural Science Youth Foundation of Heilongjiang Province (No. QC2016011) and the Innovation Fund for Graduate Students of Harbin Normal University

Compliance with ethical standards

Conflict of interest The authors declare that they have no competing interests.

References

- Agostinis P, Berg K, Cengel KA, Foster TH, Girotti AW, Gollnick SO (2011) Photodynamic therapy of cancer: an update. *CA Cancer J Clin* 61:250–281
- Allison RR, Mota HC, Bagnato VS, Sibata CH (2008) Bio-nanotechnology and photodynamic therapy—state of the art review. *Photodiagn Photodyn Ther* 5:19–28
- Altieri DC (2001) The molecular basis and potential role of Survivin in cancer diagnosis and therapy. *Trends Mol Med* 7:542–547
- Asano R, Nagami A, Fukumoto Y, Yazama F, Ito H, Sakata I, Tai A (2013) Synthesis and biological evaluation of new chlorin derivatives as potential photosensitizers for photodynamic therapy. *Bioorg Med Chem* 21:2298–2304
- Ashikaga T, Wada M, Kobayashi H, Mori M, Katsumura Y, Fukui H, Kato S, Yamaguchi M, Takamatsu T (2000) Effect of the photocatalytic activity of TiO₂ on plasmid DNA. *Mutat Res* 466:1–7
- Belfield KD, Bondar MV, Przhonska OV (2005) Singlet oxygen quantum yield determination for a fluorene-based two-photon photosensitizer. *J fluoresc* 16:111–117
- Berneburg M, Gretherbeck S, Kurten V, Ruzicka T, Briviba K, Sies H, Krutmann J (1999) Singlet oxygen mediates the UVA-induced generation of the photoaging-associated mitochondrial common deletion. *J Biol Chem* 274:15345–15349
- Bonnett R, Martínez G (2002) Photobleaching of compounds of the 5, 10, 15, 20-Tetrakis (m-hydroxyphenyl) porphyrin series (m-THPP, m-THPC, and m-THPBC). *Org Lett* 4:2013–2016
- Buytaert E, Dewaele M, Agostinis P (2007) Molecular effectors of multiple cell death pathways initiated by photodynamic therapy. *Biochim Biophys Acta* 1776:86–107
- Cabuy E (2012) Photodynamic therapy in cancer treatment. *Reliable cancer therapies. Energy based Ther* 3:1–54

- Cheng J, Li W, Tan G, Wang Z, Li S, Jin Y (2017) Synthesis and in vitro photodynamic therapy of chlorin derivative 13¹-ortho-trifluoromethyl-phenylhydrazine modified pyropheophorbide-a. *Biomed Pharmacother* 87:263–273
- Dewaele M, Verfaillie T, Martinet W, Agostinis P (2010) Death and survival signals in photodynamic therapy. *Methods Mol Biol* 635:7–33
- Eichwurz I, Stiel H, Röder B (2000) Photophysical studies of the pheophorbide a dimer. *J Photochem Photobiol B* 54:194–200
- Garg H, Suri P, Gupta JC, Talwar GP, Dubey S (2016) Survivin: a unique target for tumor therapy. *Cancer Cell Int* 16:49–63
- Guo M, Mao H, Li Y, Zhu A, He H, Yang H, Wang Y, Tian X, Ge C, Peng Q, Wang X, Yang X, Chen X, Liu G, Chen H (2014) Dual imaging-guided photothermal/photodynamic therapy using micelles. *Biomaterials* 35:4656–4666
- Han GF, Wang JJ, Shim YK (2001) The bromination on methyl pyropheophorbide-a for constructing chlorin-bromine building block and its application. *J Photosci* 8:71–73
- Hu J, Tang Y, Elmenoufy AH, Xu H, Cheng Z, Yang X (2015) Nanocomposite-based photodynamic therapy strategies for deep tumor treatment. *Small* 11:5860–5887
- Ivanov AS, Boldyrev AI (2014) Deciphering aromaticity in porphyrinoids via adaptive natural density partitioning. *Org Biomol Chem* 12:6145–6150
- Li J, Zhang X, Liu Y, Yoon I, Kim DK, Yin JG, Wang JJ, Shim YK (2015) Synthesis, optical properties and preliminary in vitro photodynamic effect of pyridyl and quinoxalyl substituted chlorins. *Bioorg Med Chem* 23:1684–1690
- Li J, Zhang P, Yao N, Zhao L, Wang J, Shim YK (2014) Convenient peripheral aryloxylation reactions of porphyrins and chlorophyll- a-based chlorins with benzoyl peroxide. *Tetrahedron Lett* 55(5):1086–1089
- Li Q, Wang X, Zhang K, Li X, Liu Q, Wang P (2013) DNA damage and cell cycle arrest induced by protoporphyrin IX in sarcoma 180 Cells. *Cell Physiol Biochem* 32:778–788
- Li W, Tan G, Cheng J, Zhao L, Wang Z, Jin Y (2016) A novel photosensitizer 3¹,13¹-phenylhydrazine-Mppa (BPHM) and its in vitro photodynamic therapy against HeLa cells. *Molecules* 21:558–570
- Li W, Zhu G, Li J, Wang Z, Jin Y (2016) An amidochlorin-based colorimetric fluorescent probe for selective Cu²⁺ detection. *Molecules* 21:107–117
- Liu G, Qin H, Amano T, Murakami T, Komatsu N (2015) Direct fabrication of the graphene-based composite for cancer phototherapy through graphite exfoliation with a photosensitizer. *ACS Appl Mater Inter* 7:23402–23406
- Lu K, He C, Lin W (2014) Nanoscale metal-organic framework for highly effective photodynamic therapy of resistant head and neck cancer. *J Am Chem Soc* 136:16712–16715
- Luna MC, Wong S, Gomer CJ (1994) Photodynamic therapy mediated induction of early response genes. *Cancer Res* 54:1374–1380
- Malumbres M, Barbacid M (2009) Cell cycle, CDKs and cancer: a changing paradigm. *Nat Rev Cancer* 9:153–166
- Mroz P, Yaroslavsky A, Kharkwal GB, Hamblin MR (2011) Cell death pathways in photodynamic therapy of cancer. *Cancers* 3:2516–2539
- Noimark S, Dunnill CW, Parkin IP (2013) Shining light on materials—a self-sterilising revolution. *Adv Drug Deliver Rev* 65:570–580
- Nowis D, Stokłosa T, Legat M, Issat T, Jakóbiński M, Gołąb J (2005) The influence of photodynamic therapy on the immune response. *Photodiagn Photodyn Ther* 2:283–298
- O'Connor AE, Gallagher WM, Byrne AT (2009) Porphyrin and non-porphyrin photosensitizers in oncology: preclinical and clinical advances in photodynamic therapy. *Photochem Photobiol* 85:1053–1074
- Payne JT, McCaw DL, Casteel SW, Frazier D, Rogers K, Tompson RV (1996) Pharmacokinetics of pyropheophorbide-a-hexyl ether in the dog. *Laser Surg Med* 18:406–409
- Phillips D (2010) Light relief: photochemistry and medicine. *Photochem Photobiol Sci* 9:1589–1596
- Ramallo AS, Beck S, Farinha CM, Clarke LA, Heda GD, Steiner B, Sanz JR, Gallati S, Amaral MD, Harris A, Tzetis M (2004) Methods for RNA extraction, cDNA preparation and analysis of CFTR transcripts. *J Cyst Fibros* 3:11–15
- Shammas MA, Shmookler Reis RJ, Akiyama M, Koley H, Chauhan D, Hideshima T, Goyal RK, Hurley LH, Anderson KC, Munshi NC (2003) Telomerase inhibition and cell growth arrest by G-quadruplex interactive agent in multiple myeloma. *Mol Cancer Ther* 2:825–833
- Silva EF, Schaberle FA, Monteiro CJ, Dąbrowski JM, Arnaut LG (2013) The challenging combination of intense fluorescence and high singlet oxygen quantum yield in photostable chlorins—a contribution to theranostics. *Photochem Photobiol Sci* 12:1187–1192
- Smith KM, Goff DA, Simpson DJ (1985) The meso substitution of chlorophyll derivatives: direct route for transformation of bacteriopheophorbides d into bacteriopheophorbides c. *J Am Chem Soc* 107:4946–4954
- Sosnik A, Carcaboso AM (2014) Nanomedicines in the future of pediatric therapy. *Adv Drug Deliver Rev* 73:140–141
- Sparrow JR, Zhou J, Cai B (2003) DNA is a target of the photodynamic effects elicited in A2E-Laden RPE by blue-light illumination. *Invest Ophthalmol Vis Sci* 44:2245–2251
- Staron J, Boron B, Karcz D, Szczygieł M, Fiedor L (2015) Recent Progress in chemical modifications of chlorophylls and bacteriopheophorbides for the applications in photodynamic therapy. *Curr Med Chem* 2:3054–3074
- Sun X, Leung WN (2002) Photodynamic therapy with pyropheophorbide-a methyl ester in human lung carcinoma cancer cell: efficacy, localization and apoptosis. *Photochem Photobiol* 75:644–651
- Tu S, Wai-Yin Sun R, Lin MC, Tao Cui J, Zou B, Gu Q, Kung HF, Che CM, Wong BC (2009) Gold (III) porphyrin complexes induce apoptosis and cell cycle arrest and inhibit tumor growth in colon cancer. *Cancer* 115:4459–4469
- Tuncel S, Trivella A, Atilla D, Bennis K, Savoie H, Albrieux F (2013) Assessing the dual activity of a chalcone-phthalocyanine conjugate: design, synthesis, and antivascular and photodynamic properties. *Mol Pharmacol* 10:3706–3716
- Vail SA, Evans DR, Pan W (2014) Long wavelength absorbing porphyrin photosensitizers for dye-sensitized solar cells. *US Patent US8907081 B2*, 9 Dec 2014
- Volgger V, Betz CS (2016) Photodynamic therapy in the upper aerodigestive tract. Overview and outlook. *J Biophotonics* 9:1302–1313
- Voon SH, Kiew LV, Lee HB, Lim SH, Noordin MI, Kamkaew A, Burgess K, Chung LY (2014) In vivo studies of nanostructure-based photosensitizers for photodynamic cancer therapy. *Small* 10:4993–5013
- Wan Z, Mao H, Guo M, Li Y, Zhu A, Yang H, He H, Shen J, Zhou L, Jiang Z, Ge C, Chen X, Yang X, Liu G, Chen H (2014) Highly efficient hierarchical micelles integrating photothermal therapy and singlet oxygen-synergized chemotherapy for cancer eradication. *Theranostics* 4:399–411
- Wang C, Tao H, Cheng L, Liu Z (2011) Near-infrared light induced in vivo photodynamic therapy of cancer based on upconversion nanoparticles. *Biomaterials* 32(26):6145–6154

- Wang JJ, Li JZ, Jakus J, Shim YK (2012) Synthesis of long-wavelength chlorins by chemical modification for methyl pyropheophorbide-a and their in vitro cell viabilities. *J Porphyr Phthalocyanines* 16:122–129
- Williams WV, Rosenbaum H, Weiner DB (1992) Effect of RNA concentration on cDNA synthesis for DNA amplification. *Genome Res* 2:86–88
- Yang Y, Guo Q, Chen H, Zhou Z, Guo Z, Shen Z (2013) Thienopyrrole-expanded BODIPY as a potential NIR photosensitizer for photodynamic therapy. *Chem Commun* 49:3940–3942
- Yoon HK, Lou X, Chen YC, Koo Lee YE, Yoon E, Kopelman R (2014) Nano-photosensitizers engineered to generate a tunable mix of reactive oxygen species, for optimizing photodynamic therapy, using a microfluidic device. *Chem Mater* 26:1592–1600
- Yu CL, Chen S, Zhang MH, Shen T (2001) Spectroscopic studies and photodynamic actions of hypocrellin B in liposomes. *Photochem Photobiol* 73:482–488
- Zhang LJ, Bian J, Bao LL, Chen HF, Yan YJ, Wang L, Chen ZL (2014) Photosensitizing effectiveness of a novel chlorin-based photosensitizer for photodynamic therapy in vitro and in vivo. *J Can Res Clin* 140:1527–1536
- Zhang XH, Zhang LJ, Sun JJ, Yan YJ, Zhang LX, Chen N, Chen ZL (2016) Photodynamic efficiency of a chlorophyll-a derivative in vitro and in vivo. *Biomed Pharmacother* 81:265–272
- Zimcik P, Miletin M, Kopecky K, Musil Z, Berka P, Horakova V (2007) Influence of aggregation on interaction of lipophilic, water-insoluble azaphthalocyanines with DOPC vesicles. *Photochem Photobiol* 83:1497–1504